Title

Structures of Human Phosphofructokinase-1 and Atomic Basis of Cancer-Associated Mutations

Journal

Biophysical Journal, 110(3)

ISSN

0006-3495

Authors

Webb, Bradley
Forouhar, Farhad
Szu, Fu-En
et al.

Publication Date

2016-02-01

DOI

10.1016/j.bpj.2015.11.1150

Peer reviewed

Crystal structures of human phosphofructokinase-1 reveal subunit interfaces and effects of cancer mutations

Bradley A. Webb[1*], Farhad Forouhar[2*], Fu-En Szu[2], Jayaraman Seetharaman[2], Liang Tong[2,†] and Diane L. Barber[1,†]

[1]Department of Cell and Tissue Biology, University of California, San Francisco.

[2]Department of Biological Sciences, Northeast Structural Genomics Consortium, Columbia University, New York

Running title: Crystal structures of human platelet PFK-1

* equal first authors

† co-corresponding authors

Correspondence to
Diane L. Barber, PhD
Box 0512
University of California San Francisco
San Francisco, CA 94143
FAX: 415-502-7338
Email: diane.barber@ucsf.edu

Phosphofructokinase-1 (PFK-1), the "gatekeeper" of glycolysis, is a key regulator of glucose flux, and allosteric activation and inhibition of PFK-1 by over 10 metabolites and in response to hormonal signaling fine-tune glycolytic flux to meet energy requirements[1]. Mutations inhibiting PFK-1 activity cause glycogen storage disease type VII, also known as Tarui disease[2], and mice deficient in muscle PFK-1 have decreased fat stores[3]. Additionally, PFK-1 is suggested to have important roles in dysregulated metabolism in cancer[4,5]. We report here the first structures of the mammalian PFK-1 tetramer, for the human platelet isoform (*Hs*PFKP), in complex with ATP-Mg^{2+} and ADP at 3.1 and 3.4 Å, respectively. The structures reveal substantial conformational changes in the enzyme upon nucleotide hydrolysis as well as a unique tetramer interface. Mutations of residues in this interface can affect tetramer formation, enzyme catalysis and regulation, indicating the functional importance of the tetramer. With altered glycolytic flux being a hallmark of cancers[6], these new structures allow a molecular understanding of the functional consequences of somatic PFK-1 mutations identified in human cancers. We characterized three of these mutations and show that *in vitro* they have distinct effects on allosteric regulation of *Hs*PFKP activity and when expressed in cells one mutant, D564N, significantly decreases lactate production. These data support the view that mutations in PFK-1 could contribute to dysregulated metabolism in cancers. The PFKP structural blueprint for somatic mutations as well as the catalytic site can guide therapeutic targeting of PFK-1 activity to control dysregulated glycolysis in disease.

PFK-1 catalyses the first step committing glucose to the glycolytic pathway by converting fructose 6-phosphate (F6P) to fructose 1,6-bisphosphate. Despite its critical role in glucose flux, the biologically relevant crystal structure of the mammalian PFK-1 tetramer has not been determined. Crystals of PFK-1 from rabbit skeletal muscle[7] and sheep heart[8] were reported more than 50 years ago, but were not suitable for structural analysis. Previous attempts to obtain the structure of mammalian tetrameric PFK-1 used native protein or recombinant protein generated in yeast or bacteria. A limitation of using native PFK-1 is that most mammalian tissues express all three isoforms – muscle (PFKM), liver (PFKL) and platelet (PFKP)[9]. Although there are structures of PFK from prokaryotes[10-14] and eukaryotes[15-17], including dimeric rabbit PFKM expressed in *E. coli*[15], these structures provide limited information on the catalytic interface or the conformational changes with regulation of the tetrameic mammalian enzyme.

To overcome current limitations with structural studies of human PFK-1, we produced recombinant *Hs*PFKP by using a baculovirus expression system. The recombinant enzyme, purified to homogeneity (Extended Data Fig. 1a), is tetrameric as shown by transmission electron microscopy (TEM; Fig. 1a). The activity and regulation of recombinant *Hs*PFKP, including high cooperativity for F6P, a high affinity for ATP-Mg^{2+}, and high sensitivity to ATP inhibition (Extended Data Fig. 1 b, c), was similar to previously reported mouse PFKP expressed in yeast[18].

We determined the crystal structure of the *Hs*PFKP tetramer in complex with ATP-Mg^{2+} at 3.1 Å resolution (Fig. 1b-d, Extended Data Fig. 2). The atomic model has good agreement with the crystallographic data and the expected geometric parameters (Extended Data Table 1). The asymmetric unit contained two tetramers, and the eight protomers have essentially the same conformation (with rmsd of ~0.3 Å between any pair of them, Extended Data Fig. 3). The overall

organizations of the two tetramers are slightly different, reflected in part by changes in the relative orientations of the two dimers (Extended Data Fig. 3).

Each *Hs*PFKP tetramer measures 13.8 nm by 10.3 nm, similar in size and shape to what we calculated from TEM images (Figs. 1a, 1b). The tetramer is composed of a dimer of dimers, and the interface between the two dimers is relatively small, with a buried surface area of 700 $Å^2$ for each subunit (arrow labeled "t" in Figs. 1b-c). In addition, the two dimers are oriented at an angle of ~70° with respect to one another (Fig. 1d). The two subunits of the dimer are arranged in an antiparallel orientation, confirming previous predictions[19], with a buried surface area of 1800 $Å^2$ for each subunit. The active site is located at the interface between the two subunits (arrow labeled "*c*" in Figs. 1b,1e).

The structure of *Hs*PFKP likely represents the active conformation of the enzyme. The crystal was prepared at pH 7, near the physiological pH, and residues in the active site that have been shown to have important roles in substrate binding and/or catalysis have similar conformations in the *Hs*PFKP structure (Fig. 1e). The F6P substrate, as observed in the *S. cerevisiae* PFK (*Sc*PFK) structure[15], can be readily accommodated in the *Hs*PFKP active site, and is positioned correctly relative to the ATP for catalysis. The invariant substrate binding residues His208 and Arg210 from the second protomer of the dimer are located ~6 Å away from F6P, suggesting that a closure of this region of the active site may occur upon F6P binding and catalysis. Despite the presence of 10 mM ATP during crystallization, *Hs*PFKP contains only one ATP in each subunit, bound to the catalytic site. In contrast, the dimeric rabbit PFKM structure has 3 bound adenine nucleotides in each subunit[15]; ATP bound to the catalytic site, ATP/ADP bound to the inhibitory binding site, and ADP bound to the activating binding site[20]. *Hs*PFKP was inhibited by mM concentrations of ATP and this inhibition was relieved by the addition of

ADP (Extended Data Figure 1b,c), confirming that the allosteric adenine nucleotide-binding sites are functional. Alignment with the rabbit PFKM structure demonstrated that the binding pockets are conserved in *Hs*PFKP (data not shown). We also observed the binding of two phosphate groups in each protomer at positions corresponding to the prokaryotic PFK effector sites (Extended Data Fig. 2d,e). The enzyme activity, regulation and stability of PFK-1 is controlled by binding phosphate or sulfate ions[21,22]. *Hs*PFKP displayed a loss of ATP inhibition in the presence of 10 mM sodium sulfate (Extended Data Figure 2f) suggesting that phosphate-binding and inhibitory site ATP-binding are mutually exclusive in the tetrameric structure. Additional studies will be required to address this question.

We also determined the crystal structure of *Hs*PFKP in complex with ADP at 3.4 Å resolution, at pH 7.5. The relatively low resolution of this structure precludes a detailed structural comparison with that of the ATP-Mg^{2+} complex. However, it is clear that there is a dramatic change in the relative positions of the two domains in each protomer (Fig. 2a), and especially the overall structures of the dimer and tetramer (Fig. 2b). A rotation of ~12° is observed between the subdomains of the ADP complex protomer relatively to the ATP complex, leading to an 8 Å shift in the substrate binding domain relative to the nucleotide binding domain. An effect of this conformational change is to open the catalytic site (Figs. 2c, 2d), which may play a role in the release of products. In addition, this induced conformational change upon ATP hydrolysis in the first subunit likely leads to a rotation of the fourth subunit of ADP-bound structure by ~45° with respect to the ATP-bound structure, while the relative orientation of two dimers remained the same (~70°; Fig. 2b). The conformational changes observed between the ATP and ADP complexes of *Hs*PFKP are different from those seen for the R- and T-states of bacterial PFK (Extended Data Fig. 4)[11,23].

We next tested the importance of hydrophobic and electrostatic interactions at the tetramer interface for enzyme activity (Fig. 3a). The majority of residues at the interface are hydrophobic. Tyr645 and Phe649 from the two subunits form a π-stack of four aromatic side chains in the interface, with Phe649 in the middle (Fig. 3a). Phe649 is evolutionarily conserved in metazoans, including all human isoforms, but not in yeast (Fig. 3b). In fact, while the overall organization of the *Hs*PFKP tetramer is similar to that of *Sc*PFK[15], there are significant differences in the tetramer interface between the two enzymes (Extended Data Fig. 5). Especially, a Leu residue is equivalent to Phe649 in *Sc*PFK α subunit, but this Leu residue has a completely different local environment in *Sc*PFK compared to Phe649 in *Hs*PFKP (Extended Data Fig. 5). The previously reported rabbit PFKM structure corresponds to a dimer formed through the tetramer interface (Extended Data Fig. 5c), possibly because the PFKM crystals were grown at pH 5[15].

We generated recombinant *Hs*PFKP with Phe649 mutated to Leu (Extended Data Fig. 6a) to test whether Phe649 is required for tetramer formation. Previous studies showed that PFK-1 assembles into tetramers in a concentration- and ligand-dependent manner, with allosteric activators favoring the formation of tetramers and allosteric inhibitors favoring the formation of dimers[24-26]. In a buffer containing ADP, ATP and F6P, TEM showed that wild-type (WT) *Hs*PFKP particles had the dimensions and appearance of tetramers (Figs. 3c,d). In contrast, *Hs*PFKP-F649L particles were the same width but half the length of WT, consistent with dimer formation along the catalytic interface (Fig. 3c,d; Extended Data Fig. 6b). We compared the *Hs*PFKP-F649L particles to those induced by the inhibitor citrate, which was shown to cause PFKM to form dimers[27]. In a buffer containing 1 mM citrate, we saw two sizes of particles with WT *Hs*PFKP; one with dimensions of tetramers and the other with dimensions of dimers along the catalytic interface (Fig. 3c,d; Extended Data Fig. 6c), further confirming dimer formation by

*Hs*PFKP-F649L. Compared with the wild type enzyme, the catalytic activity of *Hs*PFKP-F649L was reduced 98% (Fig. 3e). These data are the first to use a mutagenesis approach to show that tetramer formation is necessary for PFK-1 activity.

The structures suggest an electrostatic interaction at the tetramer interface between Arg613 of one subunit and Glu657 of the adjacent subunit (Fig. 3a) may also be important for enzyme function. This salt bridge was only observed in the ATP-bound structure but not in the ADP-bound *Hs*PFKP structure or dimeric rabbit PFKM structures[15], suggesting that it may contribute to maintaining an active form of the mammalian tetramer. We tested this prediction by creating the E657A mutant (Extended Data Fig. 6a). *Hs*PFKP-E657A had reduced affinity of ~4.5 mM for F6P, compared with ~0.8 mM in wild type, and an ~2-fold decrease in maximum activity (Fig. 3f, Extended Data Table 2). Our data indicate that hydrophobic interactions are essential for the formation of tetramers while electrostatic interactions are required for optimal enzyme activity.

The structure of *Hs*PFKP provides a foundation for understanding the functional effects of somatic PFK-1 mutations identified in cancers. Cancer cells rely on aerobic glycolysis, termed the Warburg effect, to provide energy and cellular building blocks required to support rapid proliferation[6]. PFK-1 activity is increased in cancer cell lines and primary tumour tisues[28] and expression of PFKP is upregulated in breast[29] and liver[30] cancers. At the same time, inhibition of PFK-1 activity by glycosylation is reported to confer a selective advantage for cancer cell growth and metastasis by redirecting carbon flow through the pentose phosphate pathway[4]. The effect of somatic mutations in PFK-1 on metabolic adaptation has not been reported. We mapped the 44 reported somatic mutations in cancers[31] that were not associated with SNPs[32] onto the structure of *Hs*PFKP (Fig. 4a, Extended Data Table 3). Additionally, analysis by Mutation Assessor[33]

predicted that 28 of these mutations, such as active site residues G129W and D175Y, would alter enzyme activity.

We selected three identified somatic mutations that might affect *Hs*PFKP activity based on our structural analysis. Arg48 interacts with a bound phosphate ion in the structure (Fig. 4b), and the R48C mutant had reduced citrate inhibition, shifting $E_{50}^{Citrate}$ from 0.4 mM for wild type to greater than 4 mM (Fig. 4d) but did not markedly change effects of ATP and F6P (Fig. 4d-f, Extended Data Table 2). An analogous mutation in PFKM has been described in Tarui disease[34], where mutation of arginine to proline or leucine causes a similar loss of citrate inhibition[20]. These data indicate that Arg48 is located in the citrate-binding site, which is occupied by the phosphate ion in the current structure[34]. A serine substitution for Asn426, located close to the catalytic interface, is predicted to disrupt interactions with the backbone carbonyls of Gln472, Gly473, and Gly474 and the main-chain amide of Ile476, which are involved in positioning a loop at the catalytic interface (Fig. 4c). The N426S mutant partially relieves ATP inhibition, shifting EC_{50}^{ATP} from ~1 mM to greater than 3 mM (Fig. 4e). Located across the catalytic interface from Asn426, Asp564 forms an electrostatic interaction with Arg319 (Fig. 4b). The D564N mutant had decreased maximum velocity and affinity for F6P (Fig. 4f, Extended Data Table 2). The distinct effects of mutations to Asp564 and Asn426 despite their proximity across the catalytic interface suggests that information is not conveyed between subunits at this location. We also stably expressed *Hs*PFKP wild type and mutants tagged with GFP in MTLn3 rat mammary adenocarcinoma cells (Extended Data 7b). In cell lysates, PFK-1 activity was greater with expression of wild type, N426S, and D564N but not R48C compared with untransfected or GFP controls (Extended Data 7c). Lactic acid excretion was also greater with cells expressing wild type and N426S but significantly less with D564N compared with GFP

controls (Fig. 4g). These data show that expression of mutant HsPFKP can alter lactate production, although the functional significance of selective somatic mutations will also depend on the mutational signature of the respective cancer in which they occur as well as the relative expression of other PFK-1 isoforms.

In addition to cancer, aberrant glycolytic flux is increasingly recognized to contribute to a number of other diseases such as obesity, diabetes and Tarui diesease. The biologically relevant tetrameric structures of the *Hs*PFKP provide information on the catalytic interface and conformational changes upon ATP hydrolysis that contributes to a mechanistic understanding of the functional impact of disease-associated mutations. Additionally, these new structural insights will enable rational drug design for therapeutic development.

Supplementary Information is linked to the online version of the paper at www.nature.com/nature.

Acknowledgments

We thank S Oakes for access to FPLC instrumentation and R Fletterick and K White for helpful discussions. This work was supported by NIH R01 GM047413 to DLB, and a CIHR postdoctoral fellowship and a Pilot/Feasibility grant from the UCSF Liver Center (P30 DK026743) to BAW, and a grant from the Protein Structure Initiative of the National Institutes of Health U54-GM094597 to LT.

Author Contributions

BAW and DLB conceived initial studies with recombinant *Hs*PFKP and initiated the crystallographic studies through a submitted proposal to the Protein Structure Initiative (PSI) that was approved. BAW expressed and purified recombinant *Hs*PFKP, performed thermostability screens to identify buffer conditions for protein stability, and submitted samples for a high throughput screen of crystallization conditions to the Hauptman-Woodward Institute (HWI). Crystallization and structural determination were performed by FF, FS, JS and LT using protein purified by BAW and conditions identified by HWI. BAW generated and biochemically characterized recombinant wild type and mutant *Hs*PFKP, and generated and analyzed cells with heterologous *Hs*PFKP expression. BAW, FF, LT and DLB contributed to writing the manuscript.

Author Information

Stuctures of ATP-Mg^{2+}- and ADP-bound *Hs*PFKP have been deposited in PDB under accession numbers (to be added upon submission), respectively. Reprints and permissions information is available at www.nature.com/reprints. The authors declare no competing financial interests. Correspondence and requests for materials should be addressed to DLB (diane.barber@ucsf.edu) and LT (ltong@columbia.edu).

References

1. Schöneberg, T., Kloos, M., Brüser, A., Kirchberger, J. & Sträter, N. Structure and allosteric regulation of eukaryotic 6-phosphofructokinases. *Biol. Chem.* **394**, 977–993 (2013).
2. Tarui, S. et al. Phosphofructokinaase deficiency in skeletal muscle. A new type of glycogenosis. *Biochem Biophys Res Commun* **19**, 517–523 (1965).
3. Getty-Kaushik, L. et al. Mice Deficient in Phosphofructokinase-M Have Greatly Decreased Fat Stores. *Obesity (Silver Spring)* (2009).doi:10.1038/oby.2009.295
4. Yi, W. et al. Phosphofructokinase 1 Glycosylation Regulates Cell Growth and Metabolism. *Science* **337**, 975–980 (2012).
5. Moreno-Sánchez, R. et al. Phosphofructokinase type 1 kinetics, isoform expression and gene polymorphisms in cancer cells. *J Cell Biochem* **113**, 1692–1703 (2012).
6. Hanahan, D. & Weinberg, R.A. Hallmarks of cancer: the next generation. *Cell* **144**, 646–674 (2011).
7. Parmeggiani, A., Luft, J.H., Love, D.S. & Krebs, E.G. Crystallization and properties of rabbit skeletal muscle phosphofructokinase. *J Biol Chem* **241**, 4625–4637 (1966).
8. Mansour, T.E., Wakid, N. & Sprouse, H.M. Studies on heart phosphofructokinase. Purification, crystallization, and properties of sheep heart phosphofructokinase. *J Biol Chem* **241**, 1512–1521 (1966).
9. Dunaway, G.A. A review of animal phosphofructokinase isozymes with an emphasis on their physiological role. *Mol Cell Biochem* **52**, 75–91 (1983).
10. Shirakihara, Y. & Evans, P.R. Crystal structure of the complex of phosphofructokinase from Escherichia coli with its reaction products. *Journal of Molecular Biology* **204**, 973–994 (1988).
11. Evans, P.R., Farrants, G.W. & Hudson, P.J. Phosphofructokinase: structure and control. *Philos Trans R Soc Lond, B, Biol Sci* **293**, 53–62 (1981).
12. Rypniewski, W.R. & Evans, P.R. Crystal structure of unliganded phosphofructokinase from Escherichia coli. *Journal of Molecular Biology* **207**, 805–821 (1989).
13. Paricharttanakul, N.M. et al. Kinetic and structural characterization of phosphofructokinase from Lactobacillus bulgaricus. *Biochemistry* **44**, 15280–15286 (2005).
14. Mosser, R., Reddy, M.C.M., Bruning, J.B., Sacchettini, J.C. & Reinhart, G.D. Redefining the role of the quaternary shift in Bacillus stearothermophilus phosphofructokinase. *Biochemistry* **52**, 5421–5429 (2013).
15. Banaszak, K. et al. The Crystal Structures of Eukaryotic Phosphofructokinases from Baker's Yeast and Rabbit Skeletal Muscle. *Journal of Molecular Biology* **407**, 284–297 (2011).
16. Sträter, N. et al. Molecular architecture and structural basis of allosteric regulation of eukaryotic phosphofructokinases. *The FASEB journal : official publication of the Federation of American Societies for Experimental Biology* **25**, 89–98 (2011).
17. Mcnae, I.W. et al. The crystal structure of ATP-bound phosphofructokinase from Trypanosoma brucei reveals conformational transitions different from those of other phosphofructokinases. *Journal of Molecular Biology* **385**, 1519–1533 (2009).
18. Sánchez-Martínez, C., Estévez, A.M. & Aragon, J.J. Phosphofructokinase C isozyme from ascites tumor cells: cloning, expression, and properties. *Biochem Biophys Res Commun* **271**, 635–640 (2000).

19. Ferreras, C., Hernández, E.D., Martínez-Costa, O.H. & Aragón, J.J. Subunit Interactions and Composition of the Fructose 6-Phosphate Catalytic Site and the Fructose 2,6-Bisphosphate Allosteric Site of Mammalian Phosphofructokinase. **284**, 9124–9131 (2009).
20. Brüser, A., Kirchberger, J., Kloos, M., Sträter, N. & Schöneberg, T. Functional linkage of adenine nucleotide binding sites in mammalian muscle 6-phosphofructokinase. *Journal of Biological Chemistry* **287**, 17546–17553 (2012).
21. Rizzo, S.C. & Eckel, R.E. Control of glycolysis in human erythrocytes by inorganic phosphate and sulfate. *Am J Physiol* **211**, 429–436 (1966).
22. Akkerman, J.W., Gorter, G., Sixma, J.J. & Staal, G.E. Human platelet 6-phosphofructokinase. Purification, kinetic parameters and the influence of sulphate ions on enzyme activity. *Biochim Biophys Acta* **370**, 102–112 (1974).
23. Schirmer, T. & Evans, P.R. Structural basis of the allosteric behaviour of phosphofructokinase. *Nature* **343**, 140–145 (1990).
24. Hesterberg, L.K. & Lee, J.C. Self-association of rabbit muscle phosphofructokinase: effects of ligands. *Biochemistry* **21**, 216–222 (1982).
25. Leite, T., Da Silva, D., Coelho, R., Zancan, P. & Sola-Penna, M. Lactate favours the dissociation of skeletal muscle 6-phosphofructo-1-kinase tetramers down-regulating the enzyme and muscle glycolysis. *Biochem J* **408**, 123 (2007).
26. Zancan, P., Marinho-Carvalho, M.M., Faber-Barata, J., Dellias, J.M.M. & Sola-Penna, M. ATP and fructose-2,6-bisphosphate regulate skeletal muscle 6-phosphofructo-1-kinase by altering its quaternary structure. *IUBMB Life* **60**, 526–533 (2008).
27. Telford, J.N., Lad, P.M. & Hammes, G.G. Electron microscope study of native and crosslinked rabbit muscle phosphofructokinase. *Proc Natl Acad Sci USA* **72**, 3054–3056 (1975).
28. Yalcin, A., Telang, S., Clem, B. & Chesney, J. Regulation of glucose metabolism by 6-phosphofructo-2-kinase/fructose-2,6-bisphosphatases in cancer. *Exp Mol Pathol* **86**, 174–179 (2009).
29. Moon, J.-S. et al. Krüppel-like factor 4 (KLF4) activates the transcription of the gene for the platelet isoform of phosphofructokinase (PFKP) in breast cancer. *Journal of Biological Chemistry* **286**, 23808–23816 (2011).
30. Park, Y.-Y. et al. Tat-activating regulatory DNA-binding protein regulates glycolysis in hepatocellular carcinoma by regulating the platelet isoform of phosphofructokinase through microRNA 520. *Hepatology* **58**, 182–191 (2013).
31. Forbes, S.A. et al. COSMIC: mining complete cancer genomes in the Catalogue of Somatic Mutations in Cancer. *Nucleic Acids Research* **39**, D945–D950 (2010).
32. 1000 Genomes Project Consortium et al. A map of human genome variation from population-scale sequencing. *Nature* **467**, 1061–1073 (2010).
33. Reva, B., Antipin, Y. & Sander, C. Predicting the functional impact of protein mutations: application to cancer genomics. *Nucleic Acids Research* **39**, e118 (2011).
34. Li, Y., Rivera, D., Ru, W., Gunasekera, D. & Kemp, R.G. Identification of allosteric sites in rabbit phosphofructo-1-kinase. *Biochemistry* **38**, 16407–16412 (1999).
35. Schindelin, J. et al. Fiji: an open-source platform for biological-image analysis. *Nat Methods* **9**, 676–682 (2012).
36. Otwinowski, Z. & Minor, W. Processing of X-ray diffraction data collected in oscillation mode. *Methods in enzymology* **276**, 307–326 (1997).
37. Vagin, A. & Teplyakov, A. Molecular replacement with MOLREP. *Acta Crystallogr. D*

Biol. Crystallogr. **66**, 22–25 (2010).
38. McRee, D.E. XtalView/Xfit--A versatile program for manipulating atomic coordinates and electron density. *Journal of Structural Biology* **125**, 156–165 (1999).
39. Brünger, A.T. et al. Crystallography & NMR system: A new software suite for macromolecular structure determination. *Acta Crystallogr. D Biol. Crystallogr.* **54**, 905–921 (1998).
40. Segall, J.E. et al. EGF stimulates lamellipod extension in metastatic mammary adenocarcinoma cells by an actin-dependent mechanism. *Clin Exp Metastasis* **14**, 61–72 (1996).
41. Lundholm, L., Mohne-Lundholm, E. & Vamos, N. Lactic acid assay with L(plus)lactic acid dehydrogenase from rabbit muscle. *Acta Physiol. Scand.* **58**, 243–249 (1963).
42. Abrantes, J.L. et al. Herpes simplex type 1 activates glycolysis through engagement of the enzyme 6-phosphofructo-1-kinase (PFK-1). *BBA - Molecular Basis of Disease* 1–9 (2012).doi:10.1016/j.bbadis.2012.04.011
43. Byrne, K.M. et al. Use of a 96-well plate reader to evaluate proliferation of equine satellite cell clones in vitro. *Methods in Cell Science* **19**, 311–316 (1998).

Figure Legends

Figure 1 – **Structure of ATP-bound tetrameric *Hs*PFKP is in the active conformation**. **a**, TEM images of *Hs*PFKP. Left panel – bar represents 50 nm. Right panel – Indicated dimensions are the mean ± SD of 37 individual particles. **b-c**, Ribbon diagrams of *Hs*PFKP displaying the relative orientation of *Hs*PFKP tetramer subunits. Each subunit is individually coloured. Arrows labeled "*c*" and "*t*" indicate the catalytic and tetramer interfaces, respectively. View in (c) is rotated 90° from (b). **d**, View rotated 90° from (c) displaying the catalytic sites. The front subunits are shown in ribbon representation and the rear subunits depicted as surface models. ATP, black; Mg^{2+}, dark green; phosphate, yellow. **e**, The binding mode of ATP-Mg^{2+} at the active site of *Hs*PFKP. The binding mode of the F6P substrate in *Sc*PFK[15] is also shown.

Figure 2 – *Hs*PFKP undergoes a large conformational change upon ATP hydrolysis. a, Structural overlay of ATP-bound (cyan) and ADP-bound (grey) *Hs*PFKP subunits. **b**, Structural overlay of ATP-bound (coloured ribbon) and ADP-bound (grey surface) *Hs*PFKP tetramers. Arrows labeled "c" and "t" represent the catalytic and tetramer interfaces, respectively. **c-d**, Conformation of the active site in the ATP-Mg^{2+}-bound (c) and ADP-bound (d) structures.

Figure 3 – Interactions at the tetramer interface of HsPFKP regulate enzyme activity. a, Interface of the *Hs*PFKP tetramer, with one of two tetramer interfaces involving residues from subunit A (cyan) and subunit D (magenta). Two views of the hydrophobic interactions at the tetramer interface and predicted electrostatic interactions between Arg613 of one subunit with Glu657 of the adjacent subunit. Arrows indicate the position of the two-fold symmetry axis in the tetramer interface, relating the two subunits. **b**, Alignment of residues from *Hs*PFKP

surrounding Phe649 (arrow) with human PFKM and PFKL and *Saccharomyces cerevisiae* PFK-1 alpha and beta subunits. **c**, TEM images of wild type (WT) and *Hs*PFKP-F649L *Hs*PFKP particles in buffer containing activator and substrates or wild type in buffer containing the inhibitor citrate. **d**, Scatter plot of length vs width for particles observed in TEM. WT with activator and substrate (black, n=53); F649L with activator and substrate (blue, n=77); WT with citrate, tetramers (green, n=76) and dimers (red, n=41). **e**, Activity of wild type *Hs*PFKP and *Hs*PFKP-F649L in buffer containing 3 mM ADP, 3 mM ATP and 8 mM F6P. Data are means ± SEM of 6 (wild type) and 9 (F649L) determinations from 2 independent protein preparations ($p < 0.001$). **f**, F6P dependence of *Hs*PFKP wild type (black squares) and E657A (grey circles) at 0.25 mM ATP. Data are means ± SEM of 8 (wild type) and 5 (E657A) determinations from 2 independent protein preparations.

Figure 4 – Somatic cancer mutations of *Hs*PFKP alter enzymatic activity and allosteric regulation. a-c, Location of indicated *Hs*PFKP mutations in human cancers identified from the COSMIC database and mapped onto the catalytic interface of the *Hs*PFKP subunit. Mutations chosen for further analysis are denoted with coloured boxes, including Arg48Cys (a, red) and location of Arg48 at PO_4^{2-}-binding site (b), Asp564Asn (a, green) and ionic bond of Asp564 with Arg319 (b), and Asn426Ser (a, blue) and location of Ans425 at the catalytic interface (c). **d-f**, The effect mutations on citrate inhibition (d), ATP activation and inhibition (e), and affinity for F6P (d). Data are means ± SEM of 3 to 4 measurements from 2 independent protein preparations for WT, black circles; Arg48Cys, red squares; Asn426Ser, red triangles; Asn564N, green triangles. **g,** Lactic acid excretion (μmol lactate excreted per hour per μg of total cell lysate) from

MTLn3 rat mammary adenocarcinoma cells expressing wild type and mutant *Hs*PFKP-GFP. Data are means ± SEM of 4 experiments. * $p < 0.05$; ** $p < 0.01$.

Methods

Cloning, expression, and purification of recombinant human PFKP.

*Hs*PFKP cDNA (NM_002627.4) encoding the 784 amino acid isoform 1 was cloned into the pFastBac HTa vector and baculovirus was generated using the Bac-to-Bac Expression system (Invitrogen, Grand Island, NY) as per manufacturer protocols. $2X10^9$ sf21 or Hi5 cells were used to express PFKP at a multiplicity of infection of 1 for 48 hours. Cell pellets were resuspended in lysis buffer (20 mM tris(hydroxymethyl)aminomethane (Tris-HCl; pH 7.5); 50 mM potassium phosphate; 1 mM 2-mercaptoethanol; 10% glycerol; 10 mM imidazole; cOmplete Protease Inhibitor Cocktail tablet (Roche)) and lysed with 15 passes of a dounce homogenizer. Cell debris was removed by centrifugation and the pellet discarded. The supernatant was incubated with Talon resin (Clontech, Mountain View, CA), washed with 20 bed volumes of lysis buffer, and eluted with a minimal volume of elution buffer (lysis buffer with 100 mM imidazole). Protein was concentrated using an Amicon Ultracel-30K Centrifugal Filter Unit (Milipore, Billerica, MA) and buffer exchanged into FPLC buffer (20 mM HEPES, pH 7.5, 100 mM KCl, 1 mM TCEP, 1 mM ATP, 1 mM $MgCl_2$, and 5 % glycerol). *Hs*PFKP was passed over a Superose 6 10/300 GL column (GE Healthcare, Piscataway, NJ) and the peak corresponding to the tetrameric fraction collected. Buffer was exchanged to crystallization buffer (20 mM HEPES, pH 7.5, 100 mM KC, 1 mM TCEP, 10 mM $MgCl_2$, and 5 % glycerol) containing either 10 mM ADP or 10 mM ATP using an Amicon Ultracel-30K Centrifugal Filter Unit and recombinant *Hs*PFKP concentrated to >5 mg/ml. Protein was stored at 4°C. Recombinant *Hs*PFKP was tested for activity and allosteric regulation prior to crystallization.

PFK-1 activity assays

Activity assays for PFK-1 were preformed using an auxiliary enzyme assay[20]. Kinetic studies were performed in 200 µl reaction containing 50 mM HEPES pH 7.4, 100 mM KCl, 10 mM $MgCl_2$, 0.15 mM NADH, 0.675 units/ml aldolase, 5 units/ml triosephosphate isomerase, and 2 units/ml glycerol phosphate dehydrogenase. ATP and fructose 6-phosphate were used as indicated. Auxiliary enzymes were desalted using an Amicon Ultracel-10K Centrifugal Filter Unit prior to use. The concentration of *Hs*PFKP was normalized and samples diluted as a 10X stock in 10% glycerol, 20mM Tris-HCl (pH 7.5) and 1mM DTT immediately prior to the assay. The temperature was equilibrated to 25ºC for 10 minutes prior to initiating the reaction with the addition of *Hs*PFKP. The absorbance at 340 nm was measured using a SpectraMax M5 microplate reader (Molecular Devices, Sunnyvale, CA). Kinetic parameters were generated by linear regression analysis of the Hill equation using Prism (GraphPad Software, La Jolla, CA) and are the average of a minimum of 3 measurements from 2 independent preparations of protein (R^2 >0.95 for all analyses). An unpaired t-test with equal variance was used to compare the activity of wild type and F649L *Hs*PFKP. One unit (U) of activity is defined as the amount of enzyme that catalyzes the formation of 1 µmol of fructose 1,6-bisphosphate per minute at 25ºC. Data on the effect of sulfate on PFK-1 activity were obtained in the presence of 10 mM sodium sulfate or 10 mM sodium chloride as a control.

Transmission Electron Microscopy

20 µl of 25 µg/ml *Hs*PFKP was applied to glow-discharged carbon-coated grids and stained with 2% (w/v) uranyl acetate. Grids were examined and photographed with a JEOL 100CX II (JEOL, Tokyo, Japan). For estimation of size of *Hs*PFKP dimers and tetramers, the length and width of individual particles from TEM images were measured using FIJI ImageJ software[35]. The average

length and width ± SD are reported. For experiments analyzing the shape and size of *Hs*PFKP for crystallography studies, the protein was diluted in TEM buffer (20 mM HEPES, pH 7.5, 100 mM KCl, 1 mM DTT, 1 mM ATP, 1 mM $MgCl_2$, and 5 % glycerol). For experiments analyzing the oligomeric state of the enzyme in the presence of activators, WT and F649L *Hs*PFKP were diluted in TEM buffer containing 3mM ADP, 3mM ATP and 8mM F6P. For experiments analyzing the oligomeric state of the enzyme in the presence of inhibitors, *Hs*PFKP was diluted in TEM buffer containing 1mM citrate.

Crystallization and structure determination

*Hs*PFKP was crystallized in two different complexes of ADP and ATP-Mg^{2+} by a microbatch method at 18°C. For the ADP complex, 2 µl of protein solution containing *Hs*PFKP (6.35 mg/ml) was mixed with 1 µl of the precipitant solution consisting of 200 mM potassium sodium tartrate tetrahydrate, pH 7.4, and 20% (w/v) PEG 3350. The same protein buffer was used for growing the crystals of the *Hs*PFKP in complex with ATP and Mg^{2+}. The crystals were obtained using microbatch method and the precipitant solution comprising 200 mM potassium thiocyanate, pH 7, and 20% (w/v) PEG 3350. All crystals were cryoprotected by addition of 20% (v/v) ethylene glycol in the respective mother liquor and flash-frozen in liquid nitrogen for data collection at 100 K.

Crystals of the *Hs*PFKP complexes both belong to space group $P2_1$. However, the crystallographic asymmetric unit of the ADP-bound form contains 4 subunits of *Hs*PFKP that are assembled as one tetramer, whereas that of ATP-Mg^{2+} form contains two tetramers. A single-wavelength native data set to resolution 3.1 Å was collected at the X4C beamline of the National Synchrotron Light Source (NSLS). The diffraction images were processed with the HKL

package[36]. The structure of PFK from rabbit skeletal muscle (PDB id: 3O8L)[15] was used to determine the ATP-Mg^{2+} structure of *Hs*PFKP using the molecular replacement method, with the program MolRep[37]. Only a monomeric model of PFK from rabbit skeletal muscle resulted in a solution, which led to structure determination of the ATP-bound *Hs*PFKP structure. The remaining of the *Hs*PFKP model was built manually with the program XtalView[38]. The structure refinement was performed with CNS[39]. A similar methodology was used for data collection and processing of the ADP-bound structure of *Hs*PFKP, the crystal of which diffracted to 3.4 Å at the X4C beamline of NSLS. The ADP-bound structure was subsequently determined using a monomeric model of the ATP-bound complex of *Hs*PFKP, with the program MolRep[37] followed by structure refinement by CNS[39]. The data processing and refinement statistics are summarized in Extended Data Table 1. The Ramachandran plots suggest that 85.4% and 74.9% of residues in ATP-bound complex and ADP-bound complex of *Hs*PFKP are in most favored regions, and there is no residue in disallowed regions, respectively.

Selection of cancer mutations and generation of point mutants.

Somatic mutations identified in human cancers were selected from the COSMIC database[31] and known SNPs were disregarded[32]. The mutations were modeled onto the structure of *Hs*PFKP and selected for further analysis. Point mutants at the tetramer interface, F649L and E657A, and cancer mutants, R48C N426S, and D564N, were generated by using a commercially available site-directed mutagenesis kit (QuikChange Lightning, Aligent, Santa Clara, CA). DNA primers were designed using the online primer design tool (http://www.genomics.agilent.com/primerDesignProgram.jsp) and purchased from Elim Biopharmaceuticals (Hayword, CA).

Analysis of cells expressing *Hs*PFKP

A mammalian *Hs*PFKP expression construct was generated by PCR amplification and the cDNA inserted into the multiple cloning site of pEGFP-N1 using the restriction enzymes XhoI and BamHI. Cancer mutations were generated by site-directed mutagenesis as described above. Constructs were expressed by transfecting MTLn3 rat mammary adenocarcinoma cells[40] using FugeneHD (Promega, Madison WI) transfection reagent. One day post-transfection cells were replated into 100 mm dishes and 800 μg/ml G418 was added to select for transfected cells. After one week of selection, FACS was used to sort cells expressing GFP. For metabolic assays, cells were seeded into a 6-well plate at a density of 3 X 10^5 cell per well. One day after replating, cells were washed twice in serum- and glutamine-free media and cells were incubated for 2 hours in 1 ml of the same media. 50 μl of the media was collected in triplicate and the amount of lactic acid in the media measured using an enzyme-linked assay[41]. 100 μl of Reagent A (300 mM hydrazine; 200 mM glycine, pH 9.5; 20 mM β-nicotinamide adenine dinucleotide) and 50 μl of Reagent B (200 U/ml L-lactate dehydrogenase from rabbit muscle (Sigma Aldrich, St. Louis MO) were added to each well and incubated for one hour at room temperature. The absorbance at 340 nm was measured and the amount of lactate was determined from a standard curve. Cells were lysed in buffer (10mM potassium phosphate, pH 7.5; 0.1% Triton X-100; cOmplete Protease Inhibitor Cocktail tablet (Roche)), cellular debris removed by centrifugation, and the protein concentration determined by the Bradford method. Lactic acid levels in the media were normalized to protein concentration. PFK-1 activity assays were preformed on the lysate as previously described[42]. Enzyme-linked PFK-1 activity assays were performed on 10 μg of total cell lysate as described above with the exception that 10 mM ammonium sulphate was added to the assay mixture and the auxiliary enzymes were not desalted. Levels of *Hs*PFKP expression

were determined by immunoblotting using rabbit anti-GFP (Invitrogen A-11122, 1DB-001-0000868907) and mouse anti-actin clone C4 (ED Millipore MAB1501, 1DB-001-0000850281) antibodies. Two-sided paired t-tests were used to determine statistical significance.

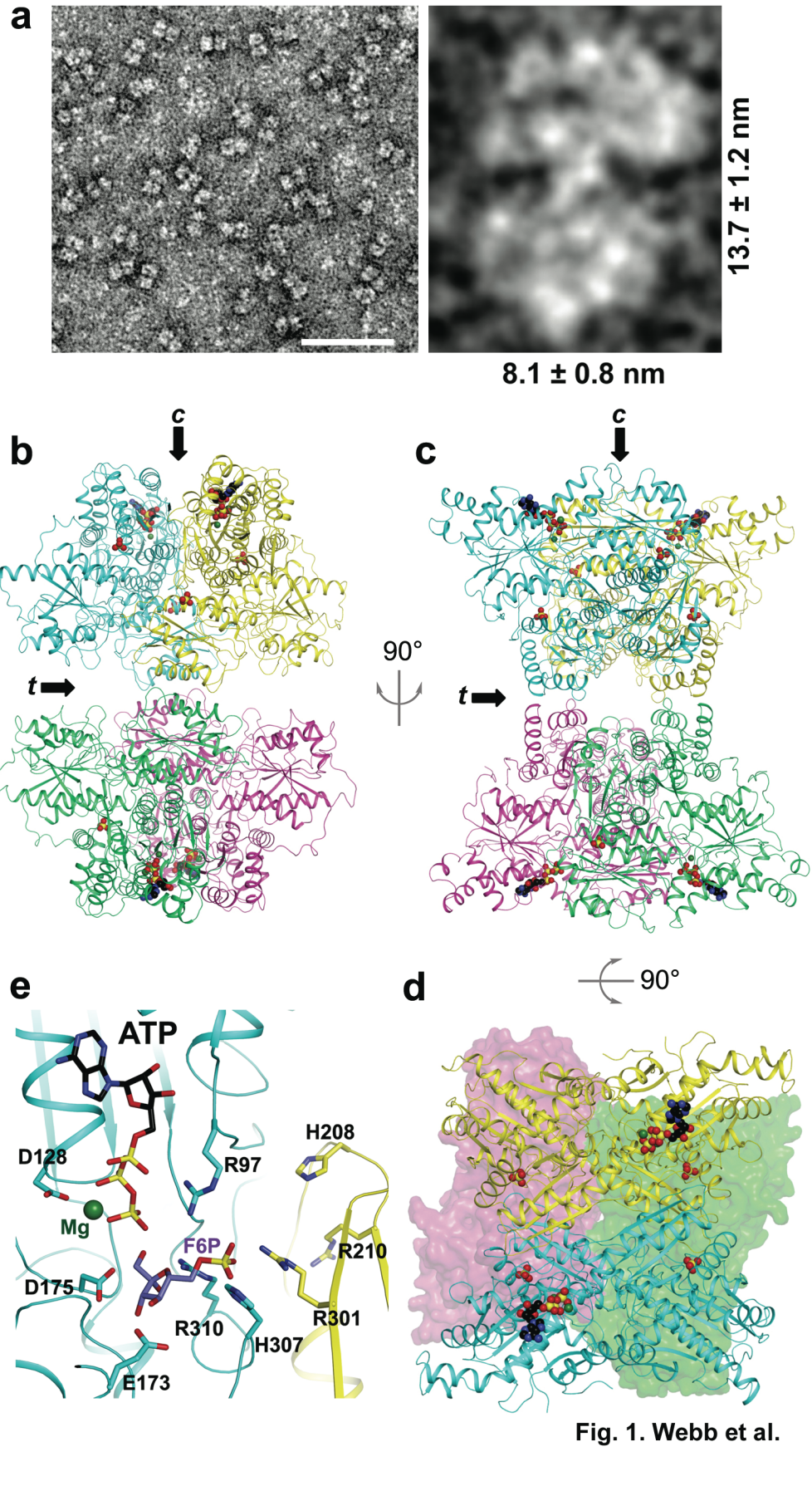

Fig. 1. Webb et al.

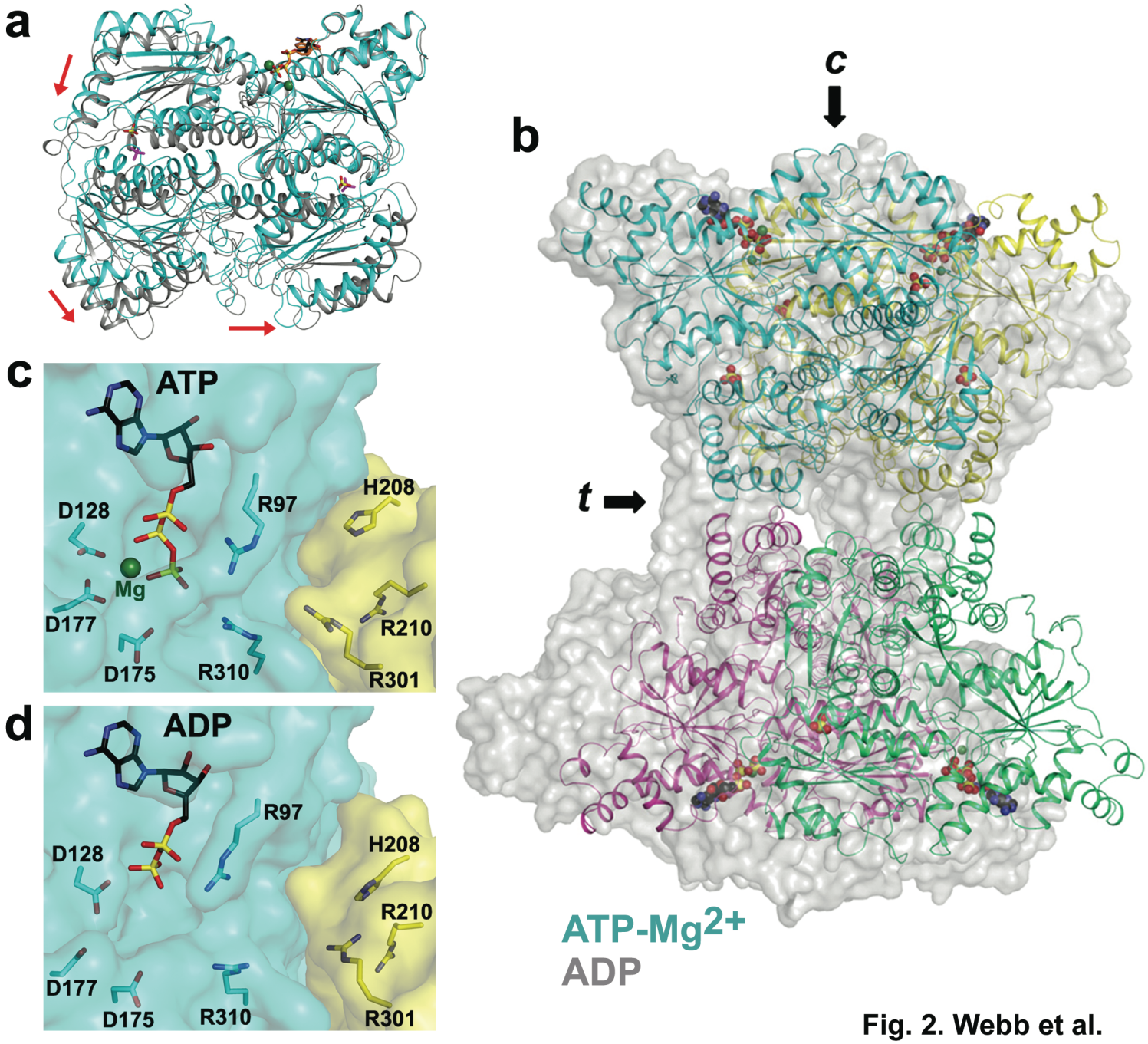

Fig. 2. Webb et al.

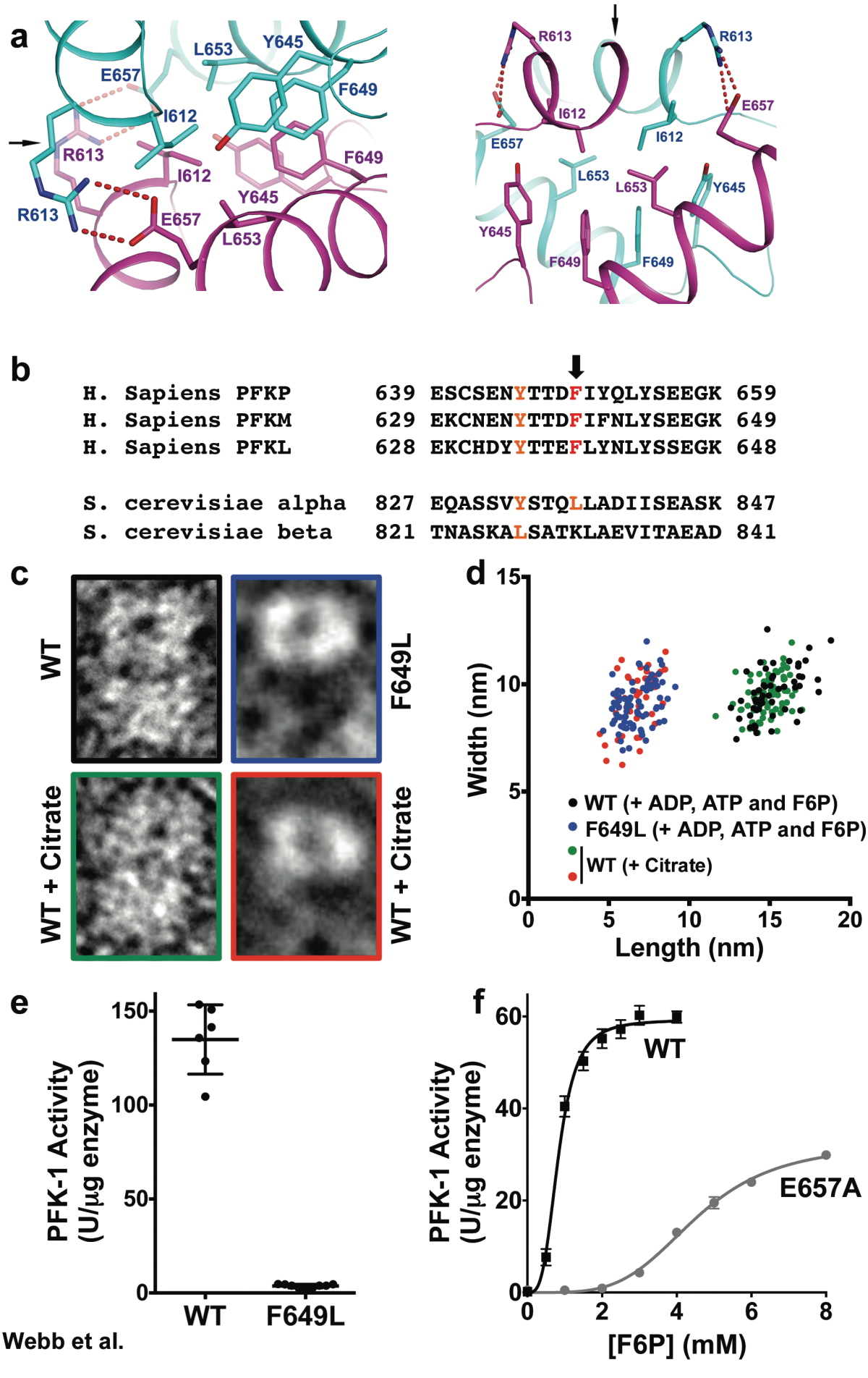

Fig. 3. Webb et al.

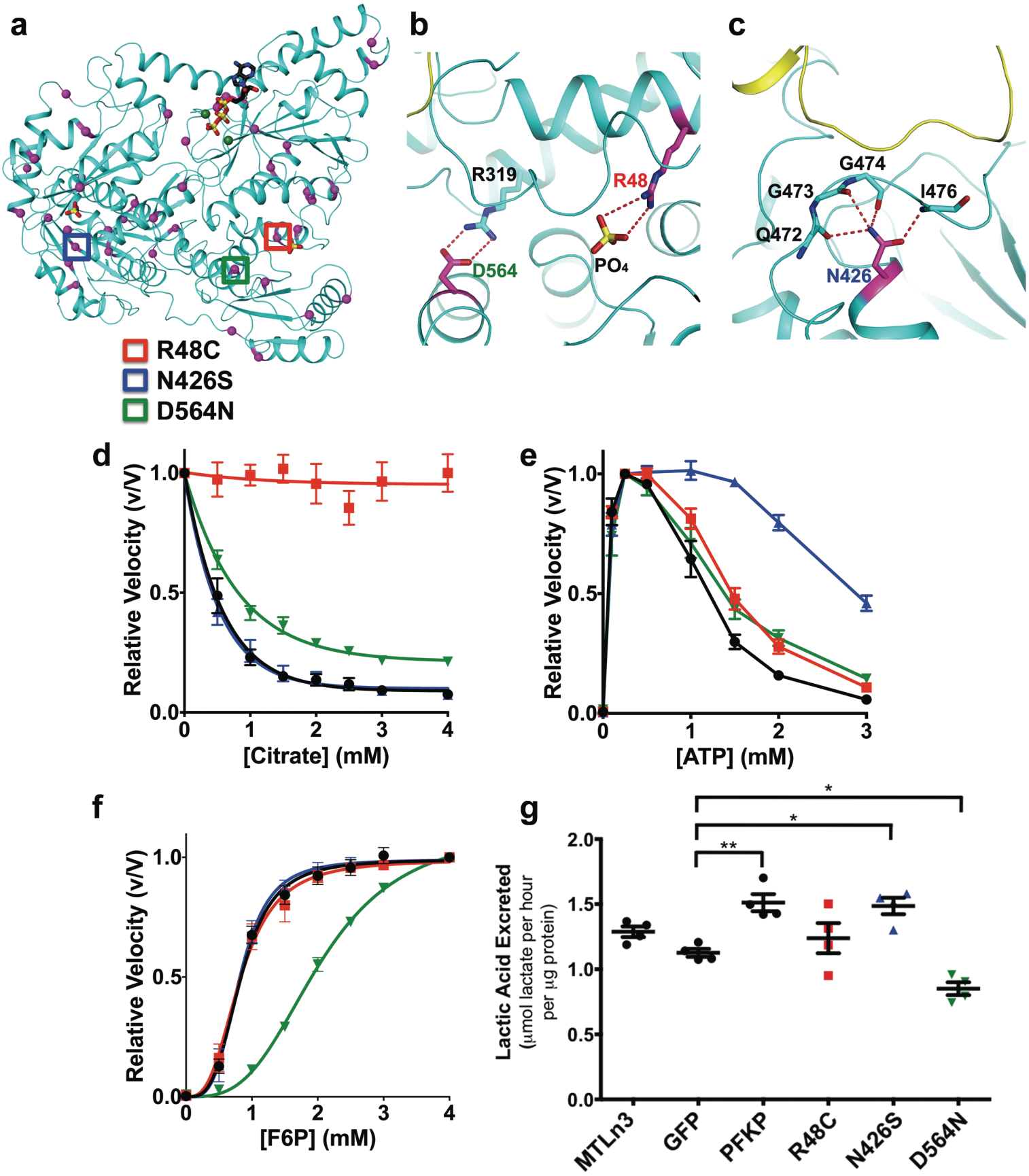

Fig. 4. Webb et al.